A Two-Step Phase Calibration Method for Tomographic Applications with Airborne SAR Data

Matteo Pardini, German Aerospace Center (DLR), matteo.pardini@dlr.de, Germany
Konstantinos Papathanassiou, German Aerospace Center (DLR), kostas.papathanassiou@dlr.de, Germany

Abstract

The extraction of accurate information from repeat-pass airborne multi-baseline (MB) synthetic aperture radar (SAR) data stacks requires a very careful phase calibration to compensate for residual baseline errors. Focusing on tomographic applications, in this paper we experiment a two-step phase calibration algorithm which is independent of the nature of scattering and can operate with an arbitrarily low number of images. In a first step, the baseline errors with respect to the master acquisition are estimated by means of a multisquint processing carried out for each single baseline with respect to the master acquisition. In a second step, the residual phase errors are compensated by means of a coherent optimization based on the minimization of the entropy of the tomographic profiles. The effectiveness of this two-step procedure is tested with MB airborne data sets acquired at different frequencies over forest and ice scenarios.

1 Introduction

SAR Tomography combines coherently (amplitude and phase) MB SAR data in order to estimate the distribution of the backscattered power along the third dimension, i.e. the height [1]. In the last years, several experiments have been carried out to analyze the effectiveness of tomographic techniques in the retrieval of the vertical structure of volumes like forests or ice. The fundamental prerequisite for any tomographic inversion is that the platform position of each track relatively to the master track is known with a precision much better than the system wavelength. However, such precision cannot be achieved by the on-board navigation instruments of airborne platforms, and the MB data stack is corrupted by phase errors induced by the resulting baseline errors. As a consequence, an accurate MB phase calibration has to be carried out prior to the tomographic focusing.

When single-baseline data are available, an effective solution has been proposed in [2], and considers multisquint processing to estimate the higher-order baseline errors followed by the detection of their linear and constant components by means of an external DEM. In the case of MB data, several calibration approaches have been proposed exploiting either stable scatterers [3, 4] or the characteristics of the scattering in the third dimension in terms of a full tomographic profile [5, 6] or of the location of its phase center [7]. The latter category of methods has several advantages: does not need to detect particular scatterers, can be applied to any natural scenario, can handle single polarization data, and it has been shown in [6] to lead to consistent tomographic reconstructions even with a low number of tracks, until the limit case of a dual-baseline acquisition.

In terms of performance, the minimization of the tomographic spectral entropy was shown in [6] to be able to reconstruct the vertical scattering profiles with at least the 90% accuracy, and to yield radiometric fidelity, a fundamental requirement for the 3-D characterization of volumes and their dynamics [8]. However, this minimization is a highly non-linear non-convex problem and needs a very careful initialization of the calibration phases. As it is shown in this paper, a way to obtain good initial calibration phases is to use the multisquint processing proposed in [2] with respect to the master acquisition. Later on, the phase calibration is refined jointly for all the baselines by minimizing the entropy of the tomographic spectra calculated in a number of cells distributed on an uniform grid in the range-azimuth plane. The performance of this two-step procedure, termed 'MuSE' (Multisquint and Spectral Entropy optimization) in the following for simplicity, is shown in this paper with reference to tomographic applications for MB airborne data sets acquired over forest and ice scenarios.

2 Basics of MuSE

Let K be the number of SAR images constituting the MB stack, and (x, y, z) the along-track (i.e. azimuth), the horizontal parallel to ground-range, and the vertical directions, respectively. For an airborne platform, the kth baseline error $\Delta B_k(r, x)$, $k = 1, \ldots, K-1$, between the master and the kth slave acquisition in the line of sight (LOS) can be written as [2, 3]:

$$\Delta B_k(r, x) = \Delta z_k(x) \cos\theta(r, x) - \Delta y_k(x) \sin\theta(r, x), \quad (1)$$

where $\Delta z_k(x)$ and $\Delta y_k(x)$ are the kth vertical and horizontal baseline errors, respectively, $\theta(r, x)$ is the local incidence angle and r is the slant-range coordinate. The resulting phase error $\phi_k(r, x)$ is given by:

$$\phi_k(r, x) = \frac{4\pi}{\lambda} \Delta B_k(r, x). \quad (2)$$

In this paper, $\phi_k(r, x)$ are compensated by means of the two-step MuSE optimization described in the following, in which model (1) is deeply exploited.

The multisquint processing estimates $\partial B_k(r,x)/\partial x$ from multiple azimuth sub-aperture interferograms between the master and the slave image, and performs integration by means of model (1) [2]. This operation outputs the higher order terms of $B_k(r,x)$, while the constant and the linear components of the baseline errors can be estimated by fitting again a model to the residual interferometric phases at each baseline, after subtraction of the synthetic interferogram generated from an external DEM [2]. It is worth noting that the usage of an external DEM automatically solves any roto-translation ambiguity of the coordinate system, and any uncertainty about target elevation is removed. We also remark that phase unwrapping is not needed in practice. In the MuSE optimization, the described multisquint and DEM fitting procedures have to be repeated for all of the available baselines independently.

After the multisquint processing has been carried out, let $\{\mathbf{y}(n)\}_{n=1}^{N}$ [1] be the K-dimensional MB complex data vectors collected in N adjacent range-azimuth pixels composing the multilook cell under test. It is reasonable to assume that the phase errors are very correlated in range and azimuth, thus it results:

$$\mathbf{y}(n) = \mathbf{y_0}(n) \odot \exp\{j\bar{\boldsymbol{\epsilon}}\}, n = 1, \ldots, N, \qquad (3)$$

where "$\odot$" denotes the Hadamard product, $\{\mathbf{y_0}(n)\}_{n=1}^{N}$ are the perfectly calibrated data vectors, $\bar{\boldsymbol{\epsilon}}$ is a K-dimensional vector defined as $\bar{\boldsymbol{\epsilon}} = [0, \boldsymbol{\epsilon}^T]^T$ in which $\boldsymbol{\epsilon}$ contains the $K-1$ residual miscalibration phases to be estimated and the 0 corresponds to the master image. Let $f(z)$ be the adaptive beam forming (i.e. Capon, ABF) profile calculated from $\{\mathbf{y}(n)\}_{n=1}^{N}$ as a function of the vertical height z in the interval of interest. It is known that in absence of miscalibration $f(z)$ shows remarkable height super-resolution, sidelobe rejection and sharpness. However, even the presence of small residual baseline errors makes $f(z)$ less sharp with higher sidelobe levels and possible height mislocations of the imaged scatterers [6, 8]. In the information theory, the sharpness of a function can be expressed by means of the Renyi entropy, which is defined as [6]:

$$S_2[f(z)] = 2\ln\sum_{m=1}^{M} f^2(z_m) - \ln\sum_{m=1}^{M} f^4(z_m), \qquad (4)$$

where z_m are the heights at which the profile is sampled. The higher $S_2[f(z)]$, the higher the entropy, and the lower the sharpness. Consequently, $\boldsymbol{\epsilon}$ can be estimated as:

$$\hat{\boldsymbol{\epsilon}} = \arg\min_{\boldsymbol{\epsilon}} S_2[f(z,\boldsymbol{\epsilon})], \qquad (5)$$

in which the dependence of $f(z)$ on $\boldsymbol{\epsilon}$ has been made explicit for the sake of clarity.

Given the high non-linearity of the minimization problem (5), $\boldsymbol{\epsilon}$ can be obtained in an iterative way through a simple gradient descent solution. In formulas, the phase error estimates at the ℓth step are:

$$\hat{\boldsymbol{\epsilon}}^{(\ell)} = \hat{\boldsymbol{\epsilon}}^{(\ell-1)} - \gamma\boldsymbol{\nabla}S_2(f, \hat{\boldsymbol{\epsilon}}^{(\ell-1)}), \qquad (6)$$

where γ is a real coefficient and $\boldsymbol{\nabla}S_2(f, \hat{\boldsymbol{\epsilon}}^{(\ell)})$ is a $(K-1)$-dimensional vector whose generic kth element corresponds to the derivative of $S_2[f(z,\boldsymbol{\epsilon})]$ with respect to $\epsilon_k = [\boldsymbol{\epsilon}]_k$ and calculated for $\hat{\epsilon}_k^{(\ell-1)}$. The calculation of $\boldsymbol{\nabla}S_2(f,\boldsymbol{\epsilon})$ can be carried out in closed form by exploiting known formulas for the derivatives of real functions of complex vectors [9].

Concerning the practical implementation of (6), a first remark is in order about the choice of the coefficient γ as a trade-off between the reduction of the number of iterations and the possibility to linearize $S_2(f,\boldsymbol{\epsilon})$ around $\hat{\epsilon}_k^{(\ell-1)}$. As no rules of thumb are available, a simple solution is to search in a small interval for the value of γ that minimizes the entropy of the reconstructed profile. This search can be carried out exhaustively on a coarse grid, and the interval limits can be set empirically by analysing a small number of pixels. A second remark regards the number of independent looks N to be used. In this case, a sensible choice is to set N as the minimum number of looks that allows a reliable inversion of the MB covariance matrix in the calculation of $\boldsymbol{\nabla}S_2(f, \hat{\boldsymbol{\epsilon}}^{(\ell-1)})$, but at the same time keeping high the sensitivity of ABF to the miscalibration residuals [8]. A third remark concerns the selection of calibration points. Indeed, $S_2[f(z)]$ is more sensitive to small variations of $\boldsymbol{\epsilon}$ if the volume does not occupy entirely the height interval in which $S_2[f(z)]$ is evaluated. Therefore, reliable calibration pixels have been selected by looking for a number of pixels for each range line at constant azimuth with higher MB ensemble coherence [3]. As a by-product, with this selection the computational complexity reduces as well.

The iterative process (6) can be stopped when $\hat{\boldsymbol{\epsilon}}^{(\ell)}$ does not change sensitively from $\hat{\boldsymbol{\epsilon}}^{(\ell-1)}$. Once a line at a fixed azimuth x_0 is completed, model (1) can be used to get rid of estimation errors dependent on the specific tomographic profiles of the processed cells [6]. Let $\boldsymbol{\epsilon}_k^r$ be the M-dimensional vector containing the phase errors at the kth baseline estimated in the M cells along range. Model (1) can be fitted in a least-square sense to $\boldsymbol{\epsilon}_k^r$ in order to estimate the horizontal and vertical residual baseline errors, obtaining the following solution:

$$\begin{bmatrix} \hat{\Delta}z_k(x_0) \\ \hat{\Delta}y_k(x_0) \end{bmatrix} = (\mathbf{A}^T\mathbf{A})^{-1}\mathbf{A}\boldsymbol{\epsilon}_k^r, \qquad (7)$$

where $\mathbf{A}$ is a $(M,2)$-dimensional matrix whose generic row is:

$$[\mathbf{A}]_{m,\cdot} = [\cos\theta(r_m,x_0), -\sin\theta(r_m,x_0)] \qquad (8)$$

for $m = 1, \ldots, M$. It is worth noting that the fitting (7) can be carried out on the estimated phases directly as far as no phase unwrapping is needed. This requirement is expected to be met as $\boldsymbol{\epsilon}_k^r$ contains only (possibly small) residual phases after the multisquint processing. Moreover, the need for estimating only two baseline error parameters ($\Delta z_k(x_0)$ and $\Delta y_k(x_0)$) allows to reduce noticeably M, with a consequential reduction of the computational load. A coordinate thinning can also be operated

[1] From here on, the dependence on (r,x) is dropped for the sake of notation simplicity.

in the azimuth direction, as the baseline error is expected to have a correlation length in the order of magnitude of 100m.

3 Experimental results

In this Section, experimental results are presented with the objective of analysing the performance of MuSE in phase calibration. Comparisons have been carried out with the calibration method based on the detection of coherent scatterers (CS) of [3]. An airborne L-band data set acquired in Spring 2009 by the DLR's E-SAR platform over the forest of Traunstein (Germany) has been processed. The data set is composed by 7 images with nominally uniform horizontal baselines between 0 and 30m. The distribution of the detected CS is quite sparse, especially in the forested areas. On the contrary, MuSE could be applied on a very dense and almost regular network of calibration points.

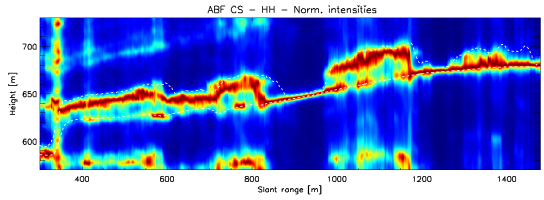

(a) ABF - After CS calibration

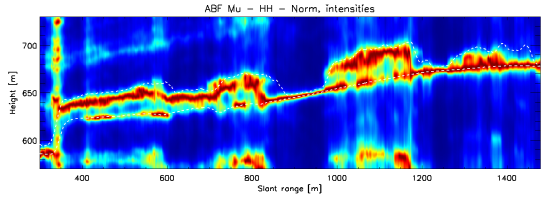

(b) ABF - After multisquint and DEM fitting

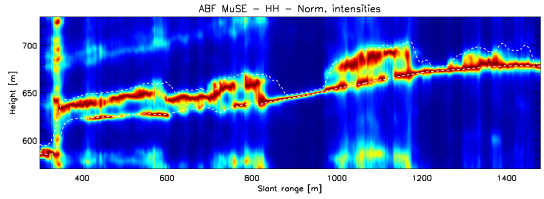

(c) ABF - After MuSE

Figure 1: Traunstein data set: calibrated intensity slices, normalized to the peak at each range. White lines: lidar ground topography and top canopy height.

Fig. 1 shows three tomographic slices in the range-height plane at the same azimuth coordinate calibrated with CS, with multisquint and DEM fitting only, and with the complete MuSE chain. Although in the three of them it is possible to locate scatterers in height consistently between the ground and the canopy top, it is apparent the superiority of MuSE. Indeed, the MuSE calibration make ABF recover its sidelobe (grating and not) suppression and super-resolution capabilities. Moreover, forest and ground layers look sharper. Comparing Fig. 1(b)-(c) it is also worth noting that the joint MB entropy optimization improves the calibration obtained by the multisquint and DEM fitting applied in a repeated single-baseline fashion.

A way to quantify the goodness of calibration is to measure the level of radiometric linearity. In fact, for single scatterers, a classical Fourier beamforming (here, BF) and ABF estimate asymptotically the same signal power. For this reason, bare areas have been selected[2] for the subsequent analysis. Fig. 2 shows the comparison between the peak intensities estimated with BF and ABF in the bare areas for the HH channel, normalized by the average power on the diagonal of the MB covariance matrix. Imaging a single scatterer, it is reasonable to expect that the normalized peak power is concentrated between 0.9 and 1, as it happens for BF. The ABF peak power is very spread with the CS calibration, with an average loss of 2.6dB. Conversely, the MuSE calibration is very effective in recovering the radiometric fidelity. Indeed, the BF and ABF peak power show a correlation higher than 0.9 and an ABF radiometric loss around 0.7dB. It is worth remarking that this loss can be further reduced by means of a very small diagonal loading (without heavily compromising height resolution) and/or by enlarging the multilook cell. The same analysis can not in general be replicated for multiple scatterers, as BF and ABF image the same structure in different ways. This is in general not a limitation for double compact scatterers spaced apart in height more than one Rayleigh resolution interval. Remarkably, in the Traunstein data set it has been found that the radiometric loss of ABF with respect to BF is around 1dB for both ground and canopy scatterer after MuSE, against the 2dB after CS calibration. Similar results have been obtained in the HV channels for both bare and forested areas.

A better calibration should also allow a more accurate polarimetric TomoSAR imaging, reducing radiometric unbalances between channels [8]. Fig. 3 shows the RGB-coded (Pauli basis) polarimetric tomogram obtained with the full-rank polarimetric ABF after MuSE in both L- and P-band. As it is reasonable to expect, ground-trunk interactions dominate the backscattered signal at P-band in most of the forested areas. At L-band, instead, clear canopy and ground signature can be well distinguished. In this case, the radiometric performance has been evaluated by calculating the normalized Frobenius norm of difference of the BF and ABF polarimetric matrices estimated in correspondence of the peak of bare areas. This difference amounts in average to less than 10% for MuSE against the (not acceptable) 20% of the CS calibration.

To complete the analysis, we considered also an ice scenario. In particular, experiments have also been carried out with an E-SAR L-band data set acquired over the Summit of Austfonna ice cap (Svalbard) during the IceSAR 2007 campaign. In this case, the nominal horizontal baselines are four and equal to 5, 10, 15 and 20m with respect to the master acquisition. It is worth noting that here number and density of the detected CS did not allow

[2]The selection has been carried out by masking out pixels with PolInSAR forest height higher than 5m.

a reliable MB phase calibration. In Fig. 4 a sample full-rank polarimetric ABF tomographic slice is shown after MuSE calibration. Reasonably, surface scattering is dominant in near range, while a sub-surface volume appears close to far range. Also in this case, phase calibration through entropy minimization turned out to improve the tomographic imaging in terms of a higher radiometric fidelity.

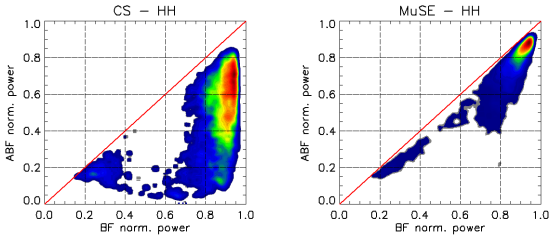

(a) After CS calibration (b) After MuSE calibration

Figure 2: Traunstein data set: comparison of the BF and ABF normalized peak intensities in bare areas.

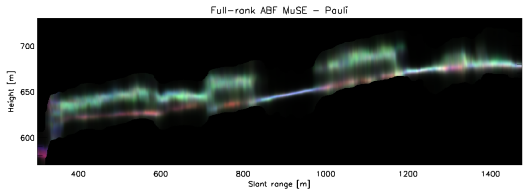

(a) ABF - L-band

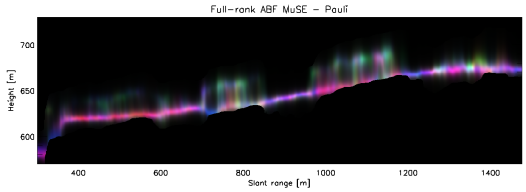

(b) ABF - P-band

Figure 3: Traunstein data set: RGB-coded (R: HH-VV, G: 2HV, B:HH+VV) full-rank polarimetric ABF tomograms, same slice of Fig. 3.

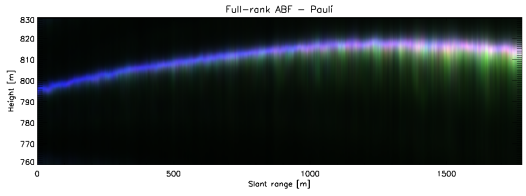

Figure 4: Summit data set: RGB-coded (R: HH-VV, G: 2HV, B:HH+VV) full-rank polarimetric ABF tomogram in the range-height plane.

4 Conclusions

In this paper, a two-step MB phase calibration algorithm called MuSE has been proposed to compensate for baseline errors in MB airborne data stacks. The experimental analysis clearly demonstrated the effectiveness of MuSE, especially in terms of recovery of height resolution, sidelobe rejection and radiometric fidelity. The most important feature of MuSE is that no MB-polarimetric scattering model is needed for calibration, which is carried out over a dense regular grid of pixels independently of the number of baselines. The MuSE calibration thus enables a very accurate 3-D imaging, fulfilling the requirements for analyses of the 3-D structure of complex natural environments (like forests and ice) and of its changes.

References

[1] A. Reigber, A. Moreira: *First Demonstration of Airborne SAR Tomography Using Multibaseline L-band Data*, IEEE Trans. on Geosci. and Rem. Sensing, Vol. 38, No. 5, pp. 2142-2152, May 2000.

[2] A. Reigber, P. Prats, J. J. Mallorqui: *Refined Estimation of Time-Varying Baseline Errors in Airborne SAR Interferometry*, IEEE Geosci. and Rem. Sensing Letters, Vol. 3, No. 1, pp. 145-149, Jan. 2006.

[3] K. Iribe, K. Papathanassiou, I. Hajnsek, M. Sato, Y. Yokota: *Coherent Scatterer in Forest Environment: Detection, Properties and its Applications*, Proc. of IEEE Int. Geosci. and Rem. Sensing Symposium, (IGARSS), Honolulu, Hawaii (USA), Jul. 2010.

[4] G. Gatti, S. Tebaldini, M. Mariotti D'Alessandro, F. Rocca: *ALGAE: A Fast Algebraic Estimation of Interferogram Phase Offsets in Space-Varying Geometries*, IEEE Trans. on Geosci. and Rem. Sensing, Vol. 49, No. 6, pp. 2343-2353, Jun. 2011.

[5] Y. Huang, L. Ferro-Famil, F. Lombardini: *Improved Tomographic SAR Focusing Using Automatic Baseline Error Compensation*, Proc. Of ESA PolInSAR Workshop, Frascati, Italy, Jan. 2011.

[6] M. Pardini, V. Bianco, K. Papathanassiou, A. Iodice: *Phase Calibration of Multibaseline SAR Data Based on a Minimum Entropy Criterion*, Proc. of IEEE Int. Geosci. and Rem. Sensing Symposium, (IGARSS), Munich, Germany, Jul. 2012.

[7] S. Tebaldini, M. Mariotti D'Alessandro, F. Banda, C. Prati: *Tomographic-Quality Phase Calibration Via Phase-Center Double Localization*, Proc. of IEEE Int. Geosci. and Rem. Sensing Symposium, (IGARSS), Melbourne, Australia, Jul. 2013.

[8] F. Lombardini, M. Pardini: *Experiments of Tomography-Based SAR Techniques With P-Band Polarimetric Data*, Proc. Of ESA PolInSAR Workshop, Frascati, Italy, Jan. 2009.

[9] D.H. Brandwood: *A Complex Gradient Operator and Its Application in Adaptive Array Theory*, IEE proceedings, Vol. 130, pts. F and H, no.1, Feb. 1983.